14 Aug 2019

Joining of Copper and Stainless Steel 304L using Direct Metal Deposition

Xinchang Zhang

Yitao Chen

Tan Pan

Wenyuan Cui

et. al. For a complete list of authors, see https://scholarsmine.mst.edu/mec_aereng_facwork/4729

JOINING OF COPPER AND STAINLESS STEEL 304L USING DIRECT METAL DEPOSITION

Xinchang Zhang*, Yitao Chen*, Tan Pan*, Wenyuan Cui*, Lan Li*, Frank Liou*

*Department of Mechanical & Aerospace Engineering, Missouri University of Science and Technology, Rolla, Missouri, 65409, USA

Abstract

In the current study, the feasibility of joining pure copper (Cu) and stainless steel 304L (SS304L) through direct metal deposition process was investigated by material characterization. Samples were analyzed in terms of microstructure, elemental distribution, and tensile testing. Direct depositing pure copper on SS304L shows copper was mechanically rather than metallurgical bonded with SS304L due to the poor dissolubility of iron in copper. Iron was diffused into copper with a diluted distance of 1.5 mm and above that, pure copper deposits were obtained. Columnar structure was observed at the copper region near the interface while the columnar grains became finer away from the interface and finally, equiaxed structure was observed. Tensile testing shows the yield strength and ultimate tensile strength of combined materials (copper and SS304L) are 123 MPa and 250 MPa and samples fractured at the copper section with a ductile fracture mechanism. The bi-material interface survived the tensile test. The yield strength and ultimate tensile strength of as-fabricated pure copper are 95.02 MPa and 186.66 MPa, respectively.

Keywords: Copper; Stainless steel 304L; Joining; Direct metal deposition

Introduction

Direct metal deposition (DMD) belongs to additive manufacturing (AM) family which utilizes a laser to melt metallic particles delivered by a powder feed nozzle. The main principle is to create a melt pool on a substrate by a laser beam and powders injected into the melt pool was melted and then solidified based on a layer by layer and track by track strategy [1]. The printing head composed of a laser and powder feed nozzle or working platform could move according to a defined route to accomplish the desired solid metallic object. DMD technology fulfills the fabrication of free-form objects, especially the geometrical complex components which are difficult to manufacture using traditional machining processes [2]. However, in addition to the creation of near end-use products, one of the most appropriate applications is for metallic component repair, especially for complex and expensive parts such as jet engine blades, dies/molds, and aircraft components [3]–[7]. For repair purpose, a certain amount of materials is delivered into the worn area to restore the missing geometry. In this way, the base parts are no longer to be discarded but can be repaired to save cost and time by replacing them.

DMD technique also has the advantage of making functionally graded materials (FGMs) [8]–[12]. DMD machine usually equipped with two or more powder feed nozzles connected to corresponding powder feeder with dissimilar materials. The materials in different feeders could be varied alloys such as stainless steel 304L (SS304L), titanium, nickel-based alloys, and cobalt-based alloys, etc. Different elemental powders could also be stored in different feeders. Since the

materials from different nozzles are different, the printed objects can be tailored by adjusting the on/off and flow rate of different feeders continuously and smoothly layer by layer. This results in changing of material composition that is a function of location, producing FGMs. FGMs are very suitable for applications that different material properties are required according to locations to accomplish better functions and properties. For example, Li et al. joined titanium alloy with SS316 through V-Cr-Fe intermediate layers to overcome potential cracking in direct joining titanium on SS316 because of forming intermetallic compounds [13]. Such FGMs possess properties of lightweight, high strength-to-weight ratio, superior heat resistance which titanium has as well as weldability and economy that SS316 could offer. SS316L and Inconel 718 FGM was fabricated in [14] and the effects of process parameters such as laser energy and powder feed rate on microstructure and mechanical properties were discussed. The result shows mechanical properties can be tailored by process parameters. Fabrication of SS304L and Inconel 625 FGM was conducted in [15]. The microstructure, phase composition, microhardness of the FGM show variation based on the volume fraction of metallic powders injected into the melt pool. Joining of SS316L and Inconel 625 was performed by inserting an intermediate layer composing of 50% SS316L and 50% Inconel 625 [16]. Many researches were concentrating on coating wear resistant alloys on components such as dies/molds and blades. For example, AISI 431 stainless steel was coated on annealed AISI A2 tool steel to improve wear and corrosion resistance [17]. A cobalt-based alloy was deposited on AISI H13 tool steel for repair worn die/mold to protect the tools from wear [18].

Copper is very attractive in certain applications because of many extremely useful properties including good electrical conductivity, great thermal conductivity, and corrosion resistance. Copper is a significant material in fabricating components such as motors, transformers, electromagnets, heat exchangers and heat sinks. Stainless steel is a cost-effective material that has a broad range of properties such as high strength and hardness, great corrosion resistance and good weldability. Joining copper with stainless steel combines the advantages of both materials. Some studies have been conducted on joining copper and stainless steel. Electron beam welding was successfully used to join copper with 304L stainless steel with no defects such as cracking [19]. Microstructure characterization reveals the fusion zone is complex because of the high cooling rate and mutually insoluble of major elements from both materials. However, the strength of the copper-stainless steel samples, especially the bi-material interface was not investigated. Explosive welding was used in [20] to join copper and stainless steel. The result shows copper can be bonded well with stainless steel with a good bonding strength and the bonding region is free of intermetallic. Joining copper with stainless steel 410 through a nickel interlayer using diffusion bonding process was investigated in [21]. Gas tungsten arc welding of copper to SS304 was performed in [22] and the result indicated the presence of defects such as cracks and lack of fusion in the bonding area. Laser welding was also applied to adhere copper with stainless steel in [23] and the microstructure and mechanical properties of the joined material were investigated.

DMD technique as an AM process was used in the present study to directly join copper with SS304L without intermediate layers. There are several issues associated with DMD processing of copper. Figure 1a shows the relationship between the reflectance of laser energy and laser wavelength for copper. It can be seen that pure copper reflects more than 95% of laser energy for lasers with about 1 μm wavelength. This indicates a very limited amount of laser radiation can be absorbed by copper, making it very difficult to melt and deposit copper. In addition to that, the

thermal conductivity of pure copper is excellent. This makes the deposition process more difficult as the small amount of energy can be quickly scattered across the whole copper substrate. Therefore, it is difficult to maintain a high temperature to stable the melt pool. One more issue is that as shown in the phase diagrams in Figure 1b [24], a very few amounts of Fe can be dissolved with Cu at room temperature, making it difficult to form Fe-Cu alloy matrix at the interface. This may cause poor bonding at the bi-material interface. Therefore, it is crucial to reveal the mechanical properties of the direct joint. Studying the dilution of Fe into Cu could reveal the gradual transition of Fe element along the thickness direction of the bonding region.

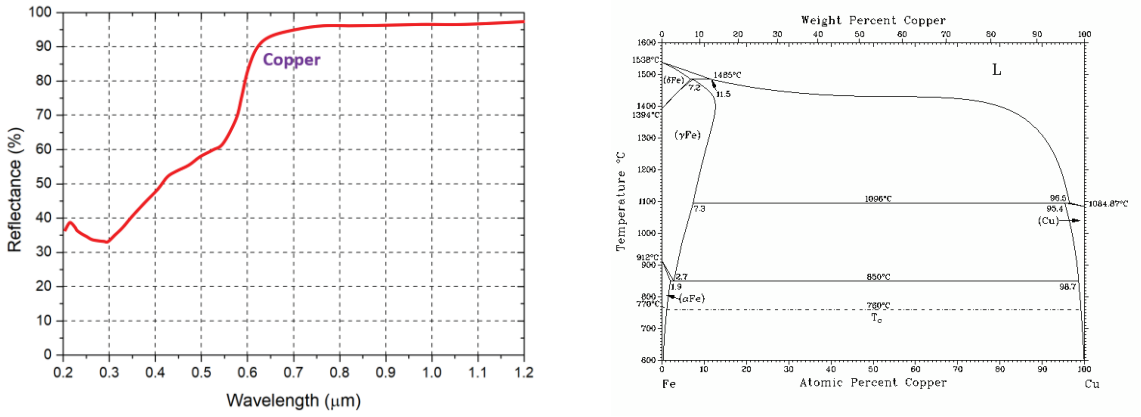

(a) (b)

Figure 1. (a) Relationship of laser reflectance with wavelength for copper; (b) Phase diagram of Fe-Cu system

Materials and experimental procedure

Gas atomized copper powder supplied by Royal Metal Powders Inc. was utilized to fabricate direct joint of copper/SS304L samples. SEM image of the copper powder was obtained as shown in Figure 2. The image reveals mostly spherical morphology although a limited number of columnar particles observed. The substrate material used in this research is SS304L with dimensions of 30 × 20 × 8 mm^3. The as-deposited copper has dimensions of 20 × 8 × 3 mm^3 (Figure 3a). The chemical composition of both materials was listed in Table 1.

A laser-assisted direct metal deposition (DMD) system was used to perform deposition of copper. The experimental setup is depicted in Figure 3b. The DMD system has a continuous wave fiber laser from IPG Photonics that can output peak power of 1000 W. The wavelength of the laser beam is ranging from 1070 nm to 1080 nm. The laser beam created a melt pool on the surface of the substrate with a spot size of 2 mm. Copper particles were delivered into the melt pool through a blown powder feeder supported by Bay State Surface Technologies, Inc. The laser beam has a tilt angle of 20° with the vertical powder feed nozzle. The ceramic powder feed nozzle has an inner diameter of 1.5 mm and a stand-off distance of 10 mm above the substrate. Argon gas was used as powder delivery gas to blow copper particles into the melt pool. The deposition process is conducted in a closed chamber filled with Argon gas as a shielding gas to prevent the processed material from oxidation. The DMD processing parameters were summarized in Table 2. For printing the first layer, a laser power of 900 W was used to create a melt pool on the substrate. After that, the laser power was reduced by 100 W each layer until the 5th layer where the laser

power was maintained at 600 W till the 8th layer. The powder flow rate is kept at 8 g/min. After printing each layer, the print table moved down by 1 mm (layer thickness) to print the next layer. The laser scanning speed was 200 mm/min.

Fabricated samples were sectioned using a wire electric discharge machine (EDM) to prepare specimens for microstructure characterization and mechanical testing. For microstructure analysis, the sliced sample was mounted on Bakelite and ground with 320, 600, 800 and 1200 grit abrasive papers, followed by polishing with 3- and 1-micron polycrystalline diamond suspension and finally polished using 0.05-micron silica suspension. The sample was etched using a solution of 10g ferric chloride, 35ml hydrochloric acid and 100ml ethanol to reveal the structure of copper grains. Optical images of the specimen were taken using a HIROX KH-8700 digital optical microscope (OM). FEI Helios NanoLab 600 DualBeam scanning electron microscope (SEM) was also used to analyze the magnified view of materials at the interface of as-deposited copper and SS304L. The SEM system equipped with Oxford Energy Dispersive Spectrometer (EDS) was utilized for elemental quantitative and distribution analysis. The dilution of elements from the substrate to as-deposited copper was analyzed.

Tensile testing and hardness measurements were performed to evaluate the mechanical properties of the fabricated samples. For obtaining tensile specimens, the as-deposited samples were sectioned to several slices with a thickness of 1.2 mm as shown in Figure 4a. After that, tensile specimens were cut from the slices according to dimensions shown in Figure 4b. In order to remove any scratches from the samples during EDM cutting, all tensile samples were ground using 600 and 800 grit abrasive papers to a thickness of approximately 1 mm. Two types of specimens were prepared: (1) samples made of as-deposited copper and SS304L substrate as shown in Figure 4c, with the bi-material interface located in the middle of the tensile gauge length. Therefore, half of the tensile specimen is copper and the remaining is SS304L. (2) samples made of pure as-deposited copper. All samples were tested using an Instron universal tester (model 5969) as shown in Figure 4d with a crosshead speed of 0.015 mm/min. Tensile stress-strain curves were obtained. Based on the tensile data, yield strength (YS) and ultimate tensile strength (UTS) of all sample were summarized. Tensile fracture morphologies in both cross-section and longitudinal section were revealed using the SEM. EDS analysis was conducted on the fracture surface to analyze elemental composition across the fracture surface.

Table 1. Chemical composition of the target materials (wt.%)

Materials	Fe	Cr	Ni	Mn	P	S	Si	N	C	Cu
Copper	-	-	-	-	-	-	-	-	-	>99.99
SS304L	Bal.	18.00-20.00	8.00-12.00	2.0 max	0.045 max	0.03 max	0.75 max	0.10 max	0.03 max	-

Table 2. DMD processing parameters for depositing copper

Laser power (W)	Powder flow rate (g/min)	Layer thickness (mm)	Scan speed (mm/min)
1st layer: 900 2nd layer: 800 3rd layer: 700 4th – 8th layer: 600	8	1	200

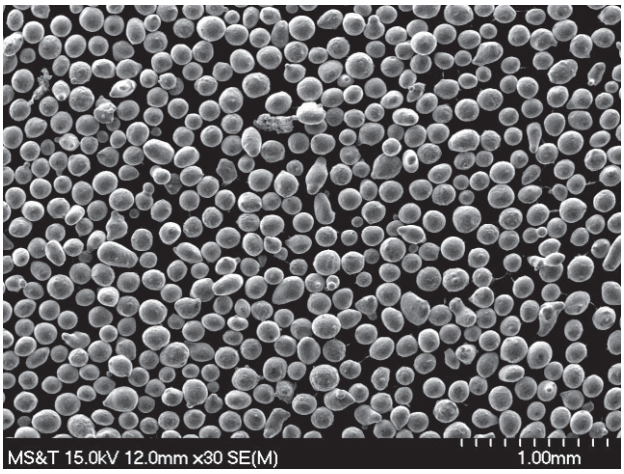

Figure 2. SEM micrograph of copper powder

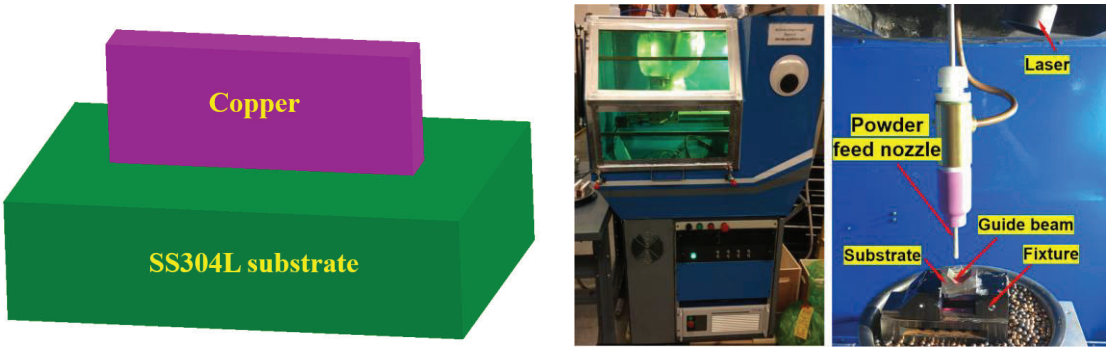

(a) (b)

Figure 3. (a) Specimen preparation of copper/SS304L direct joint; (b) DMD experimental setup

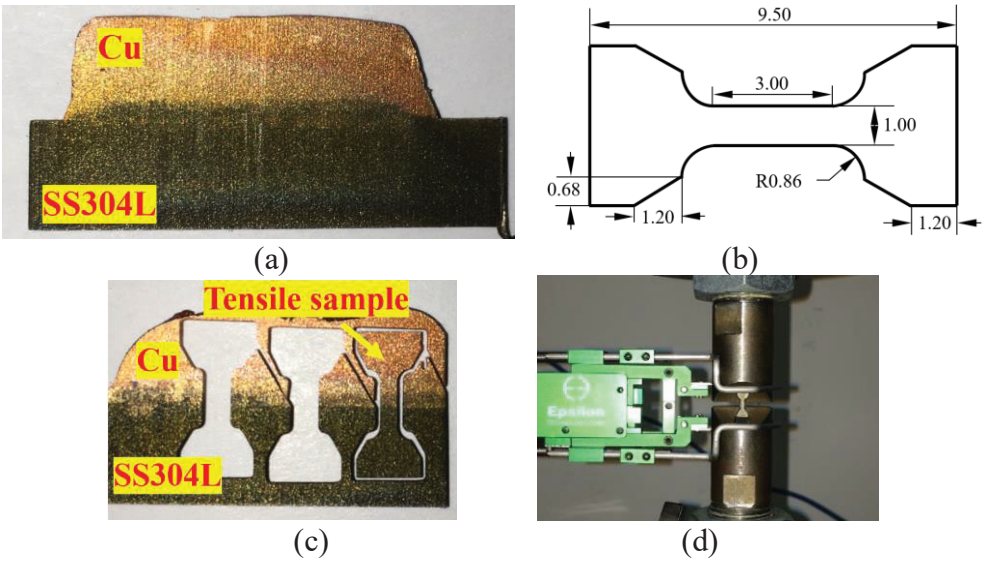

(a) (b)

(c) (d)

Figure 4. Specimen preparation for tensile testing. (a) Slices of the as-fabricated samples; (b) Tensile specimen dimensions (all dimensions in mm, 1 mm thickness); (c) Tensile samples made of copper and SS304L; (d) Tensile testing setup

Results and discussion

Microstructure characterization

The microstructure of the cross-section of the fabricated sample was analyzed as shown in Figure 5a, which shows four zones. Microstructure in zone 2, zone 3 and in the top region (zone 4) of as-deposited copper was revealed as shown in Figures 5b, 5c, and 5d, respectively. It is difficult to disclose the microstructure in zone 1 using an optical microscope and therefore scanning electron microscope was utilized and the images were shown in the following of this paper. The microstructure of copper in zone 2 and zone 3 exhibits mostly columnar structure growing towards the top of deposits and is parallel to the heat flow direction. The columnar structure is common is additively manufactured materials due to the high cooling rate associated with the deposition process. During the metal deposition, heat was generated layer by layer on the top of the substrate and the substrate functioned as a heat sink, leading to the formation of columnar structure growing opposing to the heat flux direction. The columnar grains were severely elongated because of the rapid solidification rate, leaving not enough time for forming secondary dendrites.

The microstructure images reveal that the grain size in zone 3 is much finer than that in zone 2. The average grain width in zone 2 is found to be 150 microns while is 50 microns in zone 3. This is because when printing materials in zone 3, which is the 3rd layer, because of the high thermal conductivity of copper, heat was quickly scattered and absorbed by materials in zone 2, causing the grains growing coarser. As materials building up layer upon layer, the solidification rate in the metal deposition process dropped because the temperature of the substrate was high. This caused the material in the top region of deposits featured with equiaxed structure as shown in Figure 5d.

The microstructure micrographs show the as-deposited copper is free of defects such as cracking, large gas porosities, lack of fusion, etc. It is clear to notice that the interface between copper and the substrate is very distinct because of the elemental difference between the two materials. However, the micrograph taken in the bonding area didn't exhibit issues such as delamination. The bonding strength was evaluated in tensile testing in the following of this paper and the result shows a strong bond was formed in between copper and SS304L substrate.

SEM micrographs of materials in the interfacial area and slightly above the fusion line (zone 1 in Figure 5a) were taken as shown in Figures 6a and 6b, respectively. It shows the structure on the opposite side of the bonding line is different. Above the bonding line which should be the as-deposited copper region, spherical powder-shaped objects were formed and distributed on background material. In order to understand the elemental composition of such objects as well as the background material, energy dispersive spectroscopy (EDS) was used and the results are discussed in section 3.

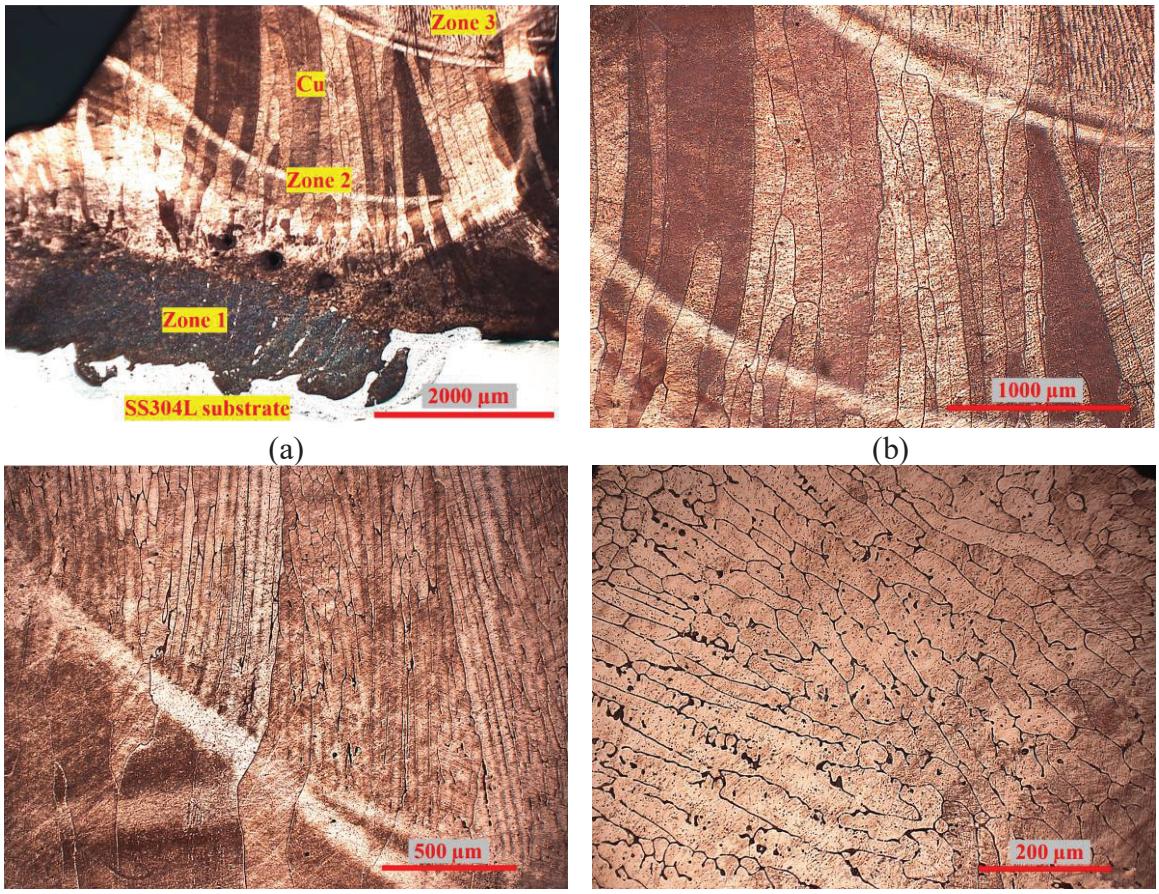

Figure 5. Optical micrographs of the longitudinal section of the sample. (a) Overview of the bonding area; (b) Magnified view of zone 2 in (a); (c) Magnified view of zone 3 in (a); (d) Magnified view of the as-deposited copper in the top region (zone 4)

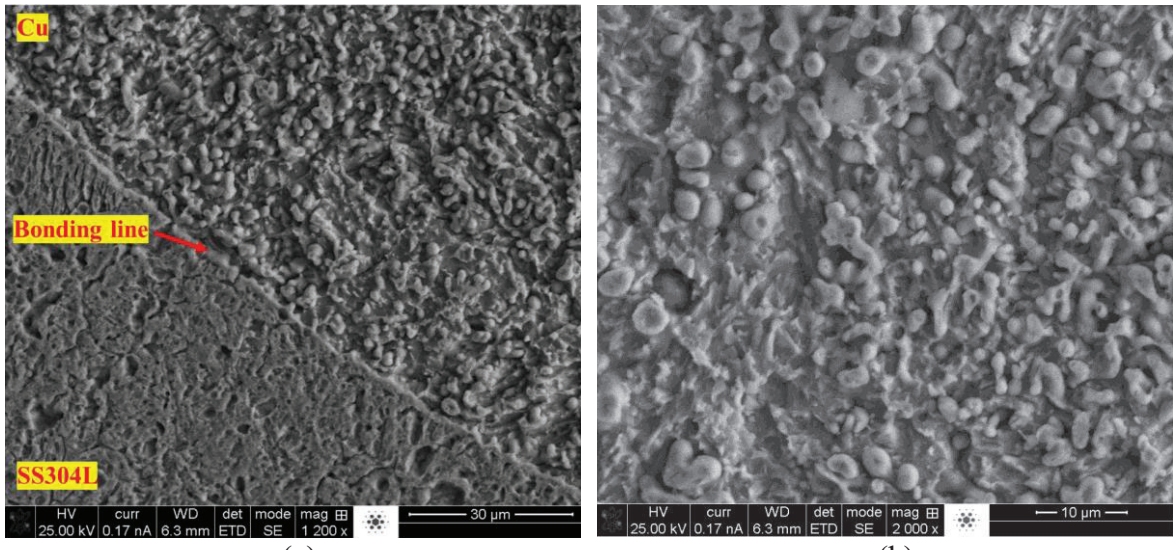

Figure 6. SEM micrographs of the longitudinal section of the sample. (a) Micrograph of material in the bonding area; (b) Micrograph of as-deposited material near the fusion line (zone 1)

EDS analysis

Figure 7 shows the EDS quantitative analysis result of materials near the interface of the substrate and the deposits. The EDS analysis was conducted on three locations: (1) spherical objects noted as spectrum 1; (2) background material depicted as spectrum 2; (3) large area marked as spectrum 3. The spectrums and elemental composition in these three locations were obtained as shown in Figures 7b-7d. Figure 7b reveals the powder-shaped material is mostly SS304L and has less amount of copper. Figure 7c shows the background material is mostly copper and very little amount of SS304L. Figure 7d shows the overview area has approximately 66% copper and 44% materials from SS304L substrate.

The result reveals the spherical material near the interface is actually SS304L material rather than unmelted copper particles. This phenomenon could be explained as follows. When additively manufacturing the first layer of deposits, laser melted the material on the top surface of the substrate, forming a melt pool. Copper particles were delivered into the melt pool and mixed with the substrate material. Because copper cannot be dissolved much in iron and chromium (major elements of SS304L) in room temperature, the substrate material precipitated and powder-shaped objects occurred. Such particles distributed in copper material due to gravity since the copper element is heavier than iron and chromium.

Figure 8 reveals the EDS mapping data of as-deposited material near the bonding line. It confirms the founding from quantitative analysis in Figure 7. Particles in Figure 8 are dominated by iron and chromium while the background material is copper. Because copper cannot dissolve much in iron and chromium, the iron/chromium and copper system will, therefore, have alternating layers of copper-rich and iron/chromium-rich materials. It also shows nickel element was evenly distributed in the inspected area. This is because copper could form a solid solution with nickel based on the phase diagram. Nickel in the SS304L substrate is mixed with copper and formed a solid solution once solidified. Because of the solid solution, nickel played a role of glue and contributed to the formation of copper/SS304L functionally graded materials.

EDS mapping is also performed on the materials across the bonding line and elemental composition and distribution are presented in Figure 8b. The result shows iron and nickel were diluted into copper deposits. Nickel is evenly distributed across the area since it can dissolve with SS304L as well as copper. Since major elements such as iron and chromium in the SS304L substrate don't readily make an alloy with copper, the as-deposited copper is mechanically but not metallurgically bonded with SS304L. In addition, because of the dilution, the as-deposited material near the interface is not pure copper, but a mixture of copper and SS304L. In order to fabricate pure copper on SS304L, the dilution distance should be analyzed, which is presented in section 4.

EDS line scan was performed on the sample from SS304L substrate to copper deposits. The result shows major elements including iron, chromium, and copper changed rapidly at the interface. However, the curves were not stable on both sides of the interface, showing rapid increasing and decreasing feature. This is because copper was not able to mix well with iron and chromium because they are not dissolvable. Therefore, alternating materials of copper and SS304L were obtained near the interface, causing the fluctuation of elemental composition.

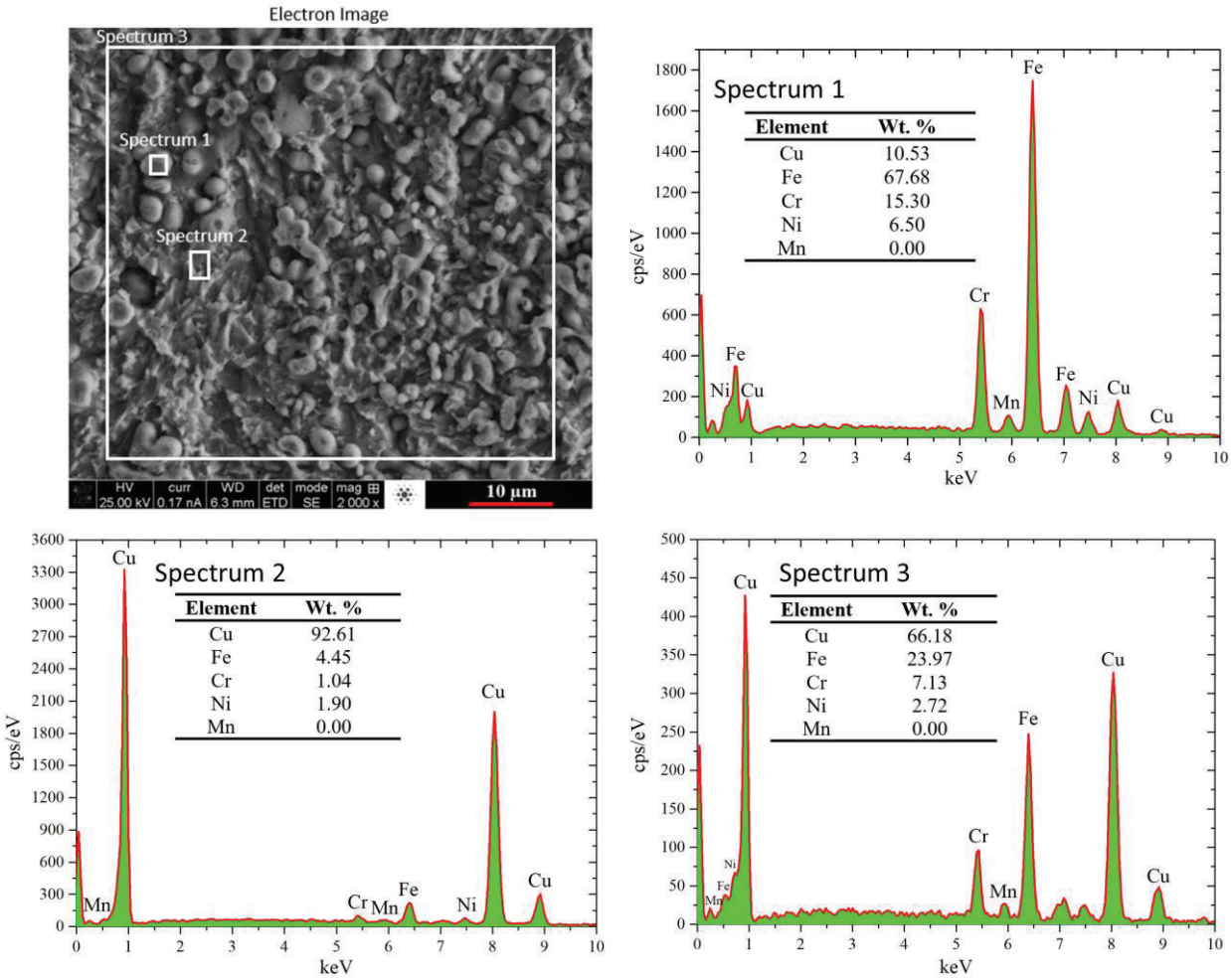

Figure 7. EDS quantitative analysis of as-deposited materials near the fusion line

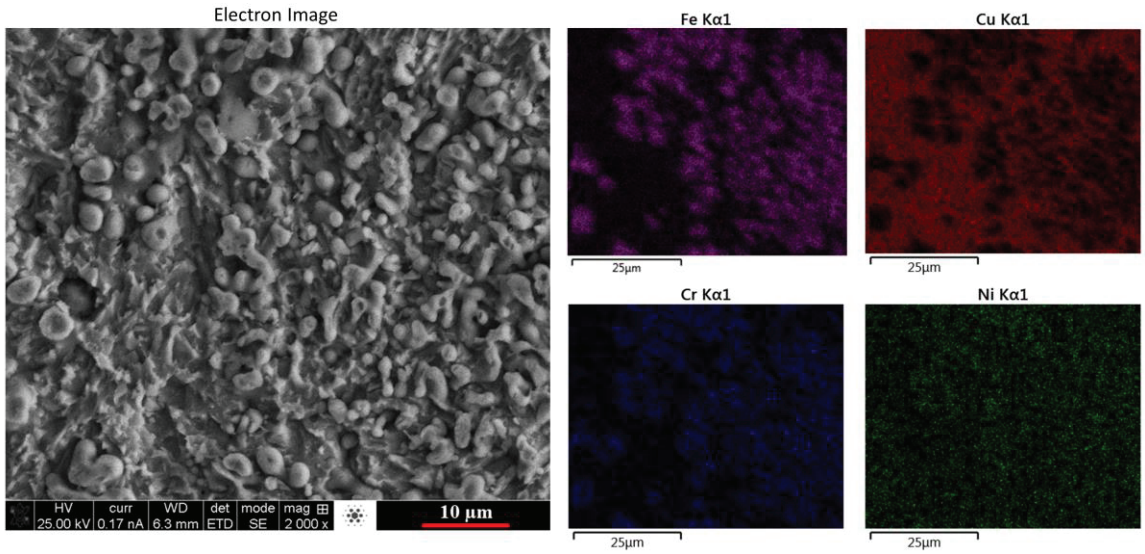

(a)

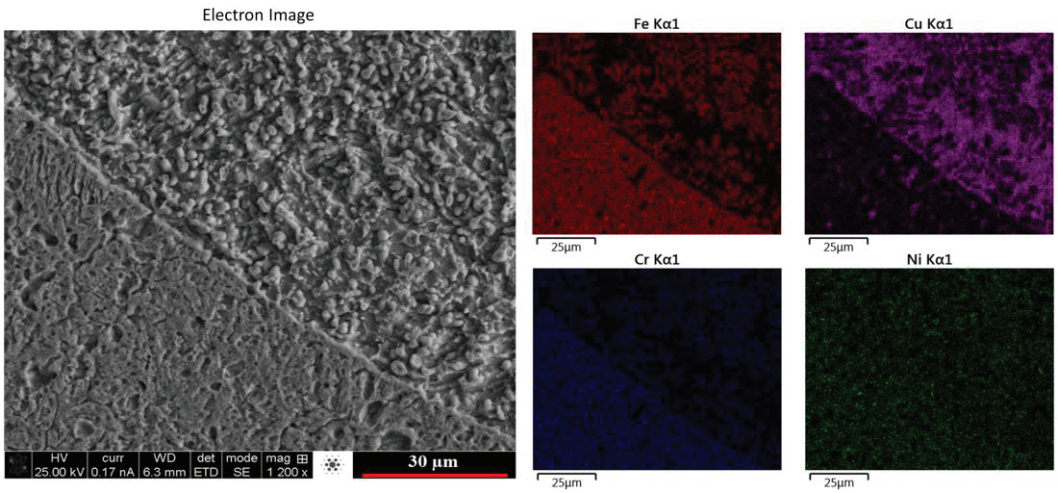

(b)

Figure 8. (a) EDS mapping of as-deposited material near the bonding line; (b) EDS mapping of as-deposited material and substrate near the bonding line

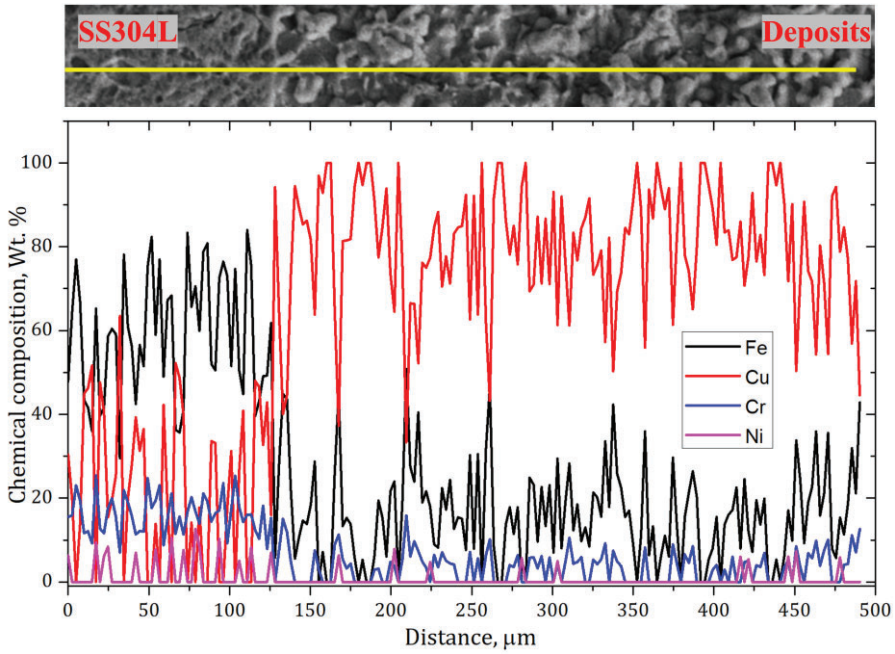

Figure 9. EDS line scan result from SS304L substrate to copper deposits

Dilution analysis

Dilution of major elements including iron, copper, chromium, nickel, and manganese was analyzed using EDS technology. EDS spectrum was taken in five locations as illustrated in Figure 10a: spectrum 1 which is below the interface, spectrum 2 which is 100 microns above the interface, spectrum 3, spectrum 4 and spectrum 5 which are 500 microns, 1000 microns, and 1500 microns above the interface, respectively. Elemental composition was quantified in these five areas and summarized in Table 3. The trend of elemental composition along the building direction is also shown in Figure 10b.

The result reveals that at spectrum 1 which is below the interface, the material is SS304L and copper didn't dilute to the area. At the spectrum 2 areas, the material is mostly made of copper and has some elements from the substrate, with the iron content of 18.67%. With the increase of the distance from the interface, copper content increased and elements from substrate decreased. Finally, at spectrum 5, the material is made of pure copper. The dilution analysis indicates that iron from the SS304L is penetrating into the as-deposited material up to 1.0 – 1.5 mm. Therefore, in order to fabricate copper on SS304L using the processing parameters described in this paper, the dimensions of deposits need to be higher than 1.5 mm to obtain pure copper deposits. This provides the information that when designing copper-SS304L FGM components to take advantage of the properties of pure copper, the thickness of deposits much meet a minimum value.

Table 3. Elemental composition of major elements in spectrums 1-5

Element	Elemental Composition, wt. %				
	Spectrum 1	Spectrum 2	Spectrum 3	Spectrum 4	Spectrum 5
Fe	71.63	18.67	7.70	1.68	0.00
Cu	0.00	73.31	88.91	98.32	100.00
Cr	19.23	5.45	2.11	0.00	0.00
Ni	7.99	2.57	1.28	0.00	0.00
Mn	1.15	0.00	0.00	0.00	0.00

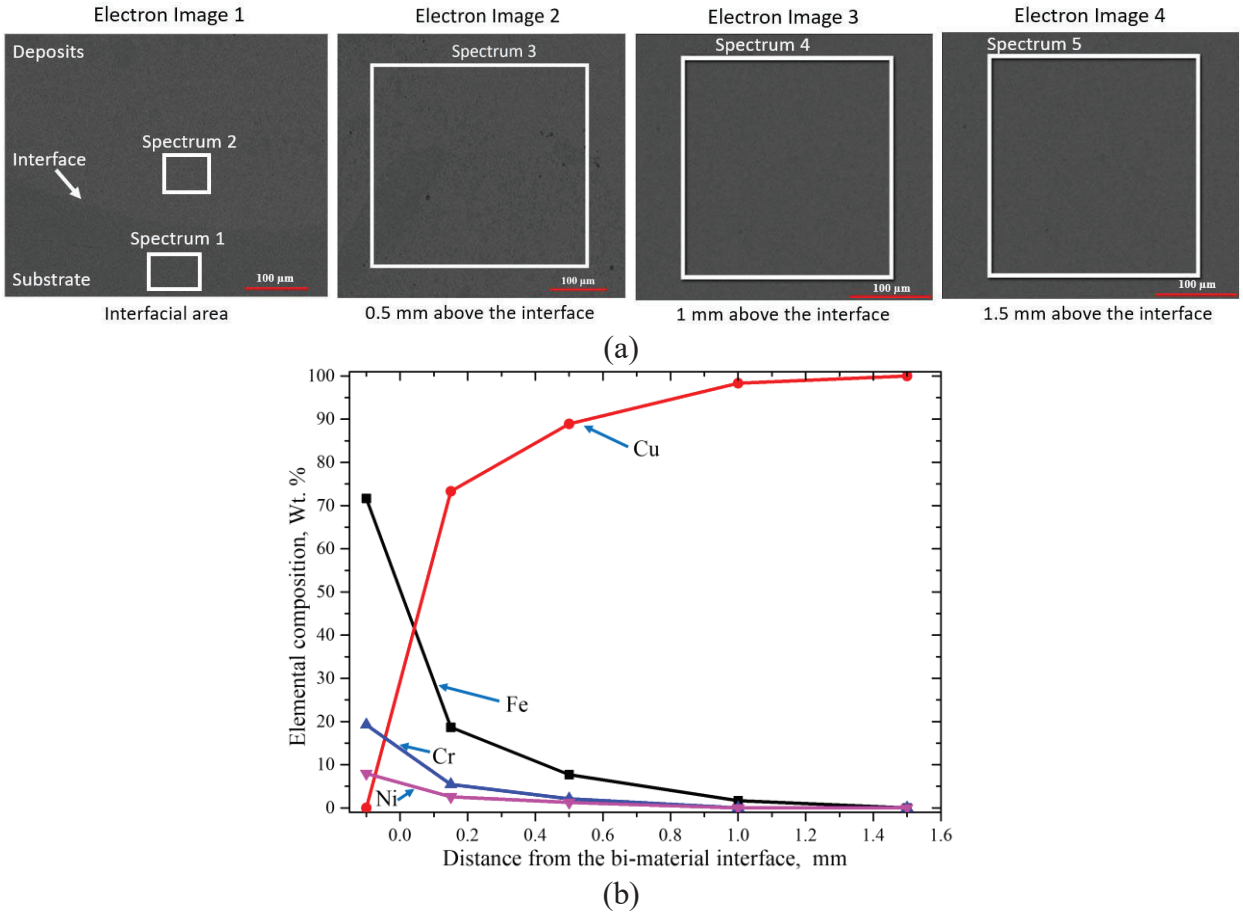

Figure 10. (a) EDS spectrums taken at five locations of the fabricated sample; (b) Relationship between the elemental composition of major elements and distance from the interface

Tensile properties

The tensile stress-strain curves of copper/SS304L and pure copper samples are plotted in Figure 11. The 0.2% offset YS, UTS, and stain at fracture are summarized in Table 4. As for copper/SS304L samples, the plots show ductile fracture mechanism since elastic deformation occurred before yielding and plastic deformation began after yielding to the maximum stress. The average YS and UTS of copper/SS304L samples were 123 MPa and 250 MPa, respectively. The strain at fracture was found to be 0.25. Tensile stress-strain curves of pure copper show the average YS and UTS of as-deposited copper is 95.02 MPa and 186.66 MPa, respectively, with the average strain at fracture of 0.58. The result shows both the YS and UTS of copper/SS304L specimens are higher than those of as-deposited pure copper. The strain curves of copper/SS304L samples show relatively inconsistent UTS and strain as plotted in Figure 11a. This might be caused by the mechanical bonding at the copper/SS304L interface. Because of the mechanical rather than metallurgical bonding, the material composition at different locations is uneven, resulting in the non-uniform stress and strain. Another reason is micro defects such as gas voids may be introduced in the printed samples, causing inconsistency of mechanical properties.

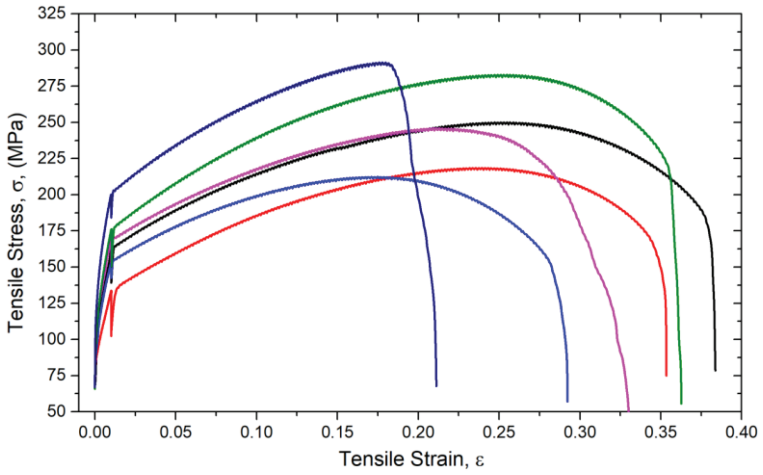

(a)

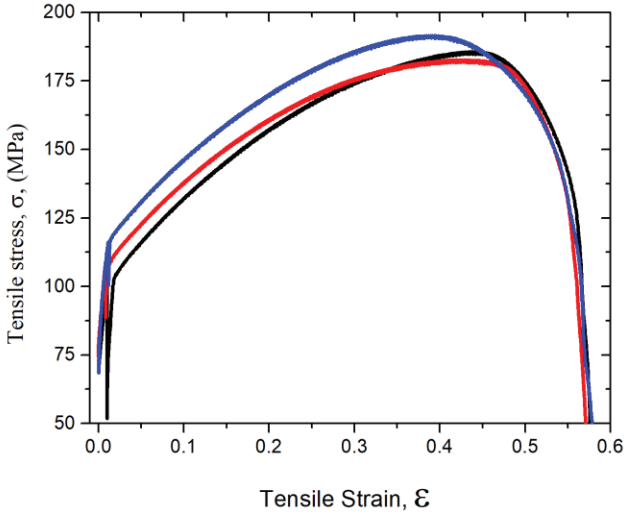

(b)

Figure 11. Tensile strain-stress curves of (a) copper+ SS304L samples and (b) copper samples

Tensile fractured specimens of copper/SS304L in longitudinal section and transverse section were analyzed using SEM and are shown in Figures 12a-b and 12c-d, respectively. The longitudinal section shows a necking was occurred in tensile testing because of the ductility of the directly joined samples. In order to understand the region where fracture happened, EDS maps were obtained. The result shows the material near the fractured region is mostly made of copper and a very small amount of chromium and nickel. Because the EDS testing comes with errors, the very little chromium and nickel content may not accurate. Therefore, tensile fracture surface in the transverse section was analyzed using EDS and depicted in Figure 12e. Quantitative analysis reveals the fracture surface is made of pure copper. This reveals the information that the copper/SS304L samples fractured at the pure copper region. This is expected because the UTS of copper is much lower than the UTS of SS304L. Therefore, during tensile testing, deformation is mostly occurred in the copper region causing the bi-materials failed at the copper section. The micrographs of fracture surface in the transverse direction (Figures 12c-d) reveal a great number of dimples which is the typical evidence of ductile fracture mechanism. Since the samples broke at the copper region, the as-deposited copper is ductile.

It was previously reported that the DMD process could form strong metallurgical bonding that can survive tensile testing, as long as the two distinct materials can be successfully joined together. In the current research, the result also shows the samples didn't fracture at the copper-SS304L interface. It shows in the microstructure analysis that copper was not metallurgically bonded with SS304L. However, the mechanical interface is still strong enough to survive the tensile testing. This could be explained that the strength of copper is lower than the interface, causing the fracture to initiate at the copper region.

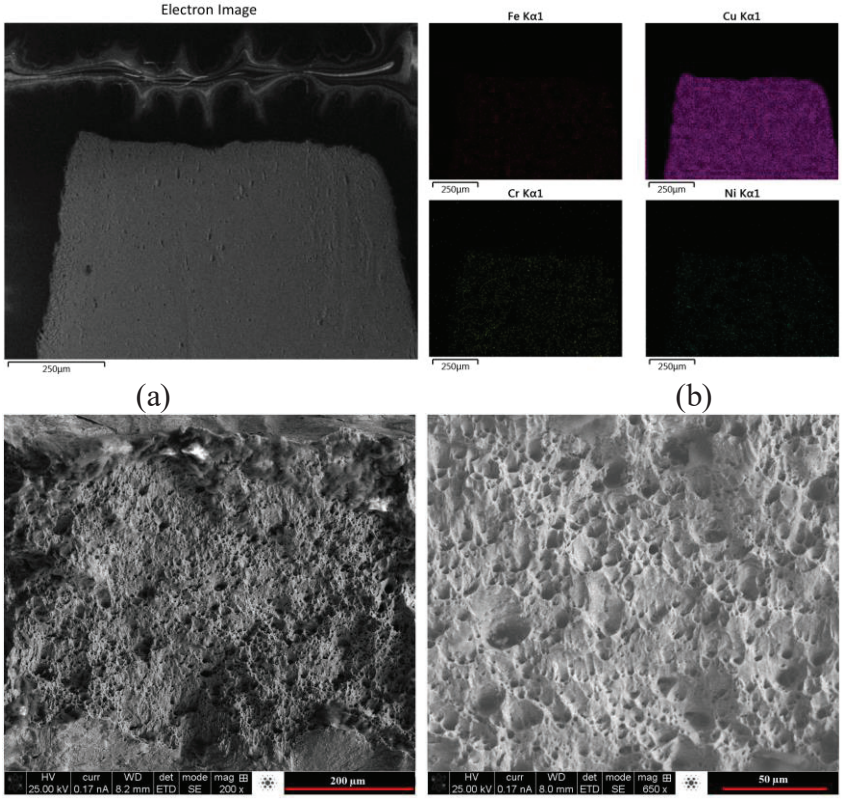

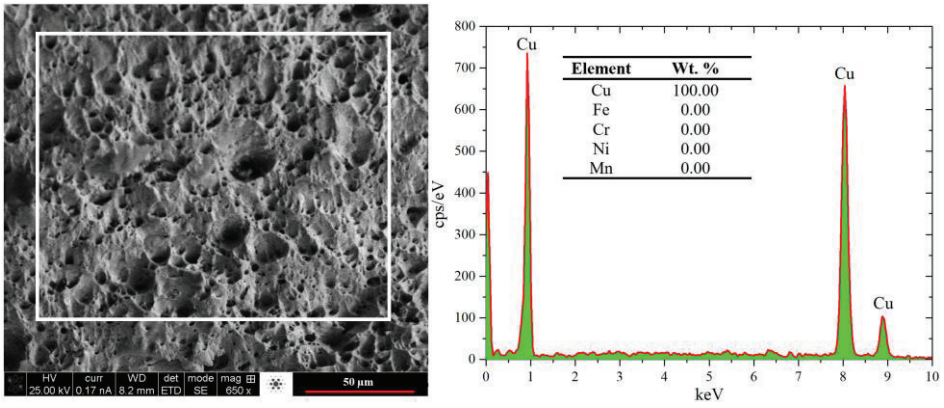

(e)

Figure 12. Tensile fracture surface morphology. (a) Overview of fracture surface in longitudinal direction; (b) EDS map of fracture surface in longitudinal direction; (c) Overview of fracture surface in transverse direction; (d) Magnified view of fracture surface in transverse direction; (e) EDS analysis of material at the fracture surface in transverse direction

Conclusion

In the present research, the feasibility of direct joining of pure copper on stainless steel 304L using direct metal deposition process was investigated. Through microstructure characterization, EDS analysis, and tensile testing, the following conclusions can be summarized.

(1) The microstructure of the cross-section of the fabricated samples shows four zones. The microstructure of Cu in zone 2 and zone 3 exhibits mostly columnar structure growing towards the top of deposits and is parallel to the heat flow direction. The columnar grains were severely elongated because of the rapid solidification rate. The grain size in zone 3 (50 µm) is much finer than that in zone 2 (150 µm) because of the dropped solidification rate. SEM micrographs of materials in zone 1 show powder-shaped objects distributed on background material.

(2) EDS analysis reveals the powder-shaped material is mostly SS304L and has less amount of Cu, and the background material is mostly Cu and very little amount of SS304L. Cu cannot be dissolved much in Fe and Cr and therefore the bonding shows alternating layers of Cu-rich and Fe/Cr-rich materials. Ni was evenly distributed in the bonding area since Cu could form a solid solution with Ni. Because of the solid solution, Ni plays the role of glue and contributes to the formation of Cu/SS304L joints. EDS line scan performed from SS304L substrate to Cu deposits shows Fe, Cr and Cu changed rapidly at the interface while the curves were not stable because Cu was not able to mix well with Fe and Cr.

(3) Dilution analysis reveals that with the increase of the distance from the interface, Cu content increases and elements from substrate decrease. The dilution analysis indicates that Fe from the SS304L was penetrating into the as-deposited Cu up to 1.0 – 1.5 mm, and above that, pure Cu was obtained.

(4) Tensile testing of combined Cu/SS304L samples shows the average YS and UTS were 123 MPa and 250 MPa, respectively. The strain at fracture was 0.25. Tensile testing of as-deposited

pure copper shows the average YS and UTS is 95.02 MPa and 186.66 MPa, respectively, with the average strain at fracture of 0.58. The result shows both the YS and UTS of Cu/SS304L specimens are higher than those of as-deposited pure Cu. Study of tensile fracture surface confirms Cu/SS304L samples failed at Cu region. The micrographs of fracture surface in transverse direction reveal a great number of dimples showing the ductile fracture mechanism of Cu. The result also shows the samples didn't fracture at the Cu-SS304L interface, revealing the solid interfacial bonding.

Acknowledgment

This project was supported by National Science Foundation Grants CMMI-1547042 and CMMI-1625736, Toyota, Intelligent Systems Center (ISC), Center for Aerospace Manufacturing Technologies (CAMT), and Material Research Center (MRC) at Missouri S&T. Their financial support is greatly appreciated.

Reference

[1] X. Zhang, W. Cui, W. Li, and F. Liou, "Effects of tool path in remanufacturing cylindrical components by laser metal deposition," *Int. J. Adv. Manuf. Technol.*, vol. 100, no. 5, pp. 1607–1617, Feb. 2019.

[2] W. E. Frazier, "Metal Additive Manufacturing: A Review," *J. Mater. Eng. Perform.*, vol. 23, no. 6, pp. 1917–1928, Jun. 2014.

[3] L. J. Kumar and C. G. K. Nair, "Laser metal deposition repair applications for Inconel 718 alloy," *Mater. Today Proc.*, vol. 4, no. 10, pp. 11068–11077, 2017.

[4] T. Petrat, B. Graf, A. Gumenyuk, and M. Rethmeier, "Laser Metal Deposition as Repair Technology for a Gas Turbine Burner Made of Inconel 718," *Phys. Procedia*, vol. 83, pp. 761–768, 2016.

[5] X. Zhang, W. Li, K. M. Adkison, and F. Liou, "Damage reconstruction from tri-dexel data for laser-aided repairing of metallic components," *Int. J. Adv. Manuf. Technol.*, pp. 1–14, 2018.

[6] S. Nowotny, S. Scharek, E. Beyer, and K.-H. Richter, "Laser Beam Build-Up Welding: Precision in Repair, Surface Cladding, and Direct 3D Metal Deposition," *J. Therm. Spray Technol.*, vol. 16, no. 3, pp. 344–348, Sep. 2007.

[7] X. Zhang, W. Li, W. Cui, and F. Liou, "Modeling of worn surface geometry for engine blade repair using Laser-aided Direct Metal Deposition process," *Manuf. Lett.*, vol. 15, pp. 1–4, 2018.

[8] W. Li, X. Chen, L. Yan, J. Zhang, X. Zhang, and F. Liou, "Additive manufacturing of a new Fe-Cr-Ni alloy with gradually changing compositions with elemental powder mixes and thermodynamic calculation," *Int. J. Adv. Manuf. Technol.*, vol. 95, no. 1, pp. 1013–1023, Mar. 2018.

[9] W. Li, L. Yan, X. Chen, J. Zhang, X. Zhang, and F. Liou, "Directed energy depositing a new Fe-Cr-Ni alloy with gradually changing composition with elemental powder mixes and particle size' effect in fabrication process," *J. Mater. Process. Technol.*, vol. 255, pp. 96–104, 2018.

[10] X. Zhang, T. Pan, W. Li, and F. Liou, "Experimental Characterization of a Direct Metal Deposited Cobalt-Based Alloy on Tool Steel for Component Repair," *JOM*, vol. 71, no. 3, pp. 946–955, Mar. 2019.

[11] W. Cui, S. Karnati, X. Zhang, E. Burns, and F. Liou, "Fabrication of AlCoCrFeNi High-Entropy Alloy Coating on an AISI 304 Substrate via a CoFe2Ni Intermediate Layer," *Entropy*, vol. 21, no. 1, 2018.
[12] R. M. Mahamood and E. T. Akinlabi, "Laser metal deposition of functionally graded Ti6Al4V/TiC," *Mater. Des.*, vol. 84, pp. 402–410, 2015.
[13] W. Li *et al.*, "Fabrication and characterization of a functionally graded material from Ti-6Al-4V to SS316 by laser metal deposition," *Addit. Manuf.*, vol. 14, pp. 95–104, 2017.
[14] K. Shah, I. ul Haq, A. Khan, S. A. Shah, M. Khan, and A. J. Pinkerton, "Parametric study of development of Inconel-steel functionally graded materials by laser direct metal deposition," *Mater. Des.*, vol. 54, pp. 531–538, 2014.
[15] B. E. Carroll *et al.*, "Functionally graded material of 304L stainless steel and inconel 625 fabricated by directed energy deposition: Characterization and thermodynamic modeling," *Acta Mater.*, vol. 108, pp. 46–54, 2016.
[16] X. Zhang, Y. Chen, and F. Liou, "Fabrication of SS316L-IN625 functionally graded materials by powder-fed directed energy deposition," *Sci. Technol. Weld. Join.*, vol. 00, 2019.
[17] C. Navas, A. Conde, B. J. Fernández, F. Zubiri, and J. de Damborenea, "Laser coatings to improve wear resistance of mould steel," *Surf. Coatings Technol.*, vol. 194, no. 1, pp. 136–142, 2005.
[18] X. Zhang, W. Li, X. Chen, W. Cui, and F. Liou, "Evaluation of component repair using direct metal deposition from scanned data," *Int. J. Adv. Manuf. Technol.*, vol. 95, no. 9, pp. 3335–3348, Apr. 2018.
[19] I. Magnabosco, P. Ferro, F. Bonollo, and L. Arnberg, "An investigation of fusion zone microstructures in electron beam welding of copper–stainless steel," *Mater. Sci. Eng. A*, vol. 424, no. 1, pp. 163–173, 2006.
[20] A. Durgutlu, B. Gülenç, and F. Findik, "Examination of copper/stainless steel joints formed by explosive welding," *Mater. Des.*, vol. 26, no. 6, pp. 497–507, 2005.
[21] H. Sabetghadam, A. Z. Hanzaki, and A. Araee, "Diffusion bonding of 410 stainless steel to copper using a nickel interlayer," *Mater. Charact.*, vol. 61, no. 6, pp. 626–634, 2010.
[22] S. G. SHIRI, M. NAZARZADEH, M. SHARIFITABAR, and M. S. AFARANI, "Gas tungsten arc welding of CP-copper to 304 stainless steel using different filler materials," *Trans. Nonferrous Met. Soc. China*, vol. 22, no. 12, pp. 2937–2942, 2012.
[23] S. Chen, J. Huang, J. Xia, X. Zhao, and S. Lin, "Influence of processing parameters on the characteristics of stainless steel/copper laser welding," *J. Mater. Process. Technol.*, vol. 222, pp. 43–51, 2015.
[24] G. Phanikumar, S. Manjini, P. Dutta, K. Chattopadhyay, and J. Mazumder, "Characterization of a continuous CO2 laser-welded Fe-Cu dissimilar couple," *Metall. Mater. Trans. A*, vol. 36, no. 8, pp. 2137–2147, Aug. 2005.